Weathering and mineralogical evolution in a high Alpine soil chronosequence: A combined approach using SEM–EDX, cathodoluminescence and Nomarski DIC microscopy

Mavris, Christian ; Götze, Jens ; Plötze, Michael ; Egli, Markus

DOI: https://doi.org/10.1016/j.sedgeo.2012.04.008

Weathering and mineralogical evolution in a high Alpine soil chronosequence: a combined approach using SEM-EDX, cathodoluminescence and Nomarski DIC microscopy

Christian Mavris[1]*, Jens Götze[2], Michael Plötze[3], Markus Egli[1]

[1] Department of Geography, University of Zurich, Winterthurerstrasse 190, CH-8057 Zürich, Switzerland

[2] TU Bergakademie Freiberg, Institute of Mineralogy, Brennhausgasse 14, D-09596 Freiberg, Germany

[3] ETH Zurich, Institute for Geotechnical Engineering, Zurich, CH-8093, Switzerland

*corresponding author:
tel. +41 44 635 51 14
fax: +41 44 635 638 48
christian.mavris@geo.uzh.ch

Abstract

Physical and chemical weathering of primary minerals of granitic till in the proglacial area of Morteratsch (Switzerland) was investigated using cathodoluminescence (CL), Nomarski differential interference contrast (DIC) microscopy and scanning electron microscope (SEM-EDX). The investigated time-span ranges from 0 to 140 yr of sediment exposure. For the very early stage of weathering or soil formation only little information is available. The main aim of our investigation was consequently to see whether weathering of primary minerals can be detected in such a short time-span using for the first time for soils well-established methods as CL and Nomarski DIC microscopy in geo- and material science such. For that purpose, the fine earth fraction (< 2 mm) of topsoil samples was investigated. Some physical

weathering had taken place within 140 years. The delamination of biotite seems to increase with time. SEM and CL analyses also demonstrate early weathering of quartz by evidencing edge pits and structural bonds – such as Si-O-Si in quartz – that start to break and to transform into free radicals. K-feldspar and plagioclase contain Fe. When using Fe^{3+} as reference point (680-700 nm) to standardise the CL spectra, the Al-O^--Al defects of K-feldspar exhibit a relative decrease with time; this was not the case for plagioclase. The CL measurements showed that the investigated apatite contained REE (rare earth elements) in the crystal structure. However, none of the other techniques (DIC, SEM-EDX) were helpful in detecting any specific weathering features for apatite. In the time span of 140 years, epidote weathering was evidenced using XRD in a previous investigation and here using DIC microscopy (morphologic changes). Several mineral changes could be traced within a very short weathering sequence using the applied techniques. These changes include physical (e.g. biotite), chemical or crystal structure (K-feldspar, biotite) features. Such an analytical combination is promising, therefore, for the detection of chemical, physical and mineralogical characteristics and changes in very young glacial sediments.

Keywords: cathodoluminescence; Nomarski DIC microscopy; SEM-EDX; weathering; soil formation; proglacial area; feldspar; plagioclase; quartz; apatite

Introduction

Due to global warming, glaciers retreat and new areas are exposed to weathering. Glaciers and discontinuous permafrost in these ecosystems react sensitively to atmospheric warming because the year-round temperature of their surrounding is not greatly below their melting point (Haeberli and Beniston, 1998). The abrasive action of active ice masses produces sediments (i.e. moraines), which tend to weather as a function of their exposure time. In the chemical sense, soil development is roughly synonymous with weathering. Elemental and mineralogical compositions of soils evolve due to complex feedbacks among geochemical

and geomorphic processes within and at the boundaries of the soil layer. Geochemical processes involve dissolution, leaching, precipitation and colloidal translocation (Yoo and Mudd, 2008), whereas geomorphic processes include the conversion of parent material to soil materials and the colluvial transport of the soil materials.

It is often assumed that weathering mechanisms in cold regions are slow due to the low temperatures. The proglacial area is, however, a potential zone of a) high geochemical reactivity due to the availability of freshly-ground reactive material (subglacially derived), b) high water-to-rock ratios and contact times, c) high permeability, and d) a constant supply of dilute waters (meltwaters and rain/snowmelt) percolating through the deposits. All these factors should favour chemical weathering. There is no agreement about the velocity of reaction in proglacial areas. Anderson et al. (1997, 2000) concluded from their measurements that silicate weathering reactions in proglacial areas may be important only after a vegetation cover is established. In contrast, Wadham et al. (2001), Egli et al. (2003) and Hosein et al. (2004) suggest that glacially derived material is subjected to intense chemical weathering, starting immediately after deposition in the proglacial zone and subsequently continuing for thousands of years after glacier retreat.

Hosein et al. (2004) and Föllmi et al. (2009a,b) measured high weathering rates in proglacial areas in the Alps (10^{-15} to 10^{-13} mol biotite m^{-2} s^{-1} for a 140-270 yr-old exposed proglacial area). Biotite weathering in young soils was generally much higher than in old soils. The calculated weathering rates of biotite were several orders of magnitude higher than known field weathering rates (e.g., Swoboda-Colberg and Drever, 1993; Murphy et al., 1998). This seems to be related to the predominance of fine-grained particles (< 63 µm) in glacial sediment that are mechanically disaggregated and preferentially leached.

In general, the availability of data about weathering rates and alteration of primary rock-forming minerals in young and cold areas is scarce. The detection of changes is often limited by the choice of techniques. The combination of transmitted-light cathodoluminescence (CL), Nomarski DIC (Differential Interference Contrast) microscopy and scanning electron microscopy (SEM-EDX) can give important insights into the chemical composition and crystal

arrangement of minerals (i.e. point defects, cationic changes, etc.). Most materials have distinct luminescence properties that allow a rapid identification of phase distribution and transformation. Nomarski DIC microscopy is an optically-based technique first documented by Nomarski and Weill (1951) and Nomarski (1955). It allows the observation of micromorphological features in natural materials and/or metal alloys, and has been applied in reflected light microscopy in metallurgy and petrographic research (e.g. Pearce et al., 1987; Keevil and Walker, 1992). Despite a relatively straightforward preparation of the samples and the high amount of information that can be retrieved by the combination of CL and Nomarski DIC, their coupled application is rare (Götze and Siedel, 2004, 2007). Transmitted-light CL microscopy is a technique applied to building materials (Michalski et al., 2002; Götze and Siedel, 2007; Götze, 2009), archaeology (Lapuente et al., 2000; Götze and Siedel, 2004) and geosciences (e.g. Götze et al., 2000; 2004; Götze and Zimmerle, 2000; Richter et al., 2003).

The aim of this study is to trace mineralogical and crystallographic changes in soils that have developed across a recently exposed granitic till. For that purpose, the proglacial area of the Morteratsch glacier was selected. The combination of preferential weathering patterns and elemental depletion (for the main structure modifier elements) for primary mineral phases were taken into account.

For this purpose, CL and Nomarski DIC microscopy – well-known analytical techniques in material science but not applied so far for soil studies – analyses were performed in combination with SEM-EDX. An additional aim was consequently to test the power and suitability of these techniques for studying short-term and initial weathering processes in young soils.

Study area

The proglacial area of Morteratsch is located in Upper Engadine, SE Switzerland (Fig. 1). The valley runs in N-S direction and the current length of the exposed area is approx. 3 km. The glacier has been continuously retreating without re-advancements since the 1850s (end of the Little Ice Age; Burga, 1999). The altitude of the investigated proglacial valley ranges

from 1900 m asl to approx. 2150 m asl, with no abrupt stacks and slopes along its main axis. Geologically, the glacial till consists of granitic material. The morainic material was produced through glacial transport within a small area of relatively homogeneous parent material (Mavris et al. 2010, 2011). The proglacial area of Morteratsch is set in the Lower Austroalpine Bernina Nappe, which is mainly composed of plutonic rocks, such as granodiorites, diorites, syenites and alkaligranites. Rarerly accessory rocks such as dolomites, gabbros and serpentines are also reported (Büchi, 1994). In the investigated area, these rock types were not observed (Mavris et al. 2010, 2011). The rock units underwent greenschist facies metamorphism during the High Alpine orogenesis (Oligocene-Eocene; Trommsdorff and Dietrich, 1999). This event caused the saussuritisation of primary rock-forming plagioclases into albite, epidote and calcite (D'Amico et al., 1998).

The vegetation cover of the Morteratsch proglacial area has been studied by Burga (1999). The first flowering plants colonising the young deglaciated surfaces are scattered individuals of *Epilobium fleischeri* and *Linaria alpina* that appear after about 7 years. First plants of the community *Oxyrietum digynae* appear after c. 12 years and disappear after c. 27 years. The establishment of *Larici-Pinetum cembrae* forests takes place after about 77 years on sites where the soil is more intensely weathered (Burga, 1999). The soils are weakly developed and are mostly Lithic Leptosols (IUSS Working Group WRB, 2006; Table 1). Present climatic conditions for the Morteratsch site are 0.5 °C mean annual temperature and 1000-1300 mm mean annual precipitation.

Material and methods

Soil sampling and preparation

Soil samples were collected from 10 soil pits distributed over the whole proglacial area (Fig. 1). This procedure resulted in the collection of a soil chronosequence of surfaces ranging from 0 (starting from the glacier front or unweathered parent material) to 140 years old. Soil

profiles were excavated down to the C horizon (Table 1). For each horizon, 1–2 kg of material was collected. The parent material (t = 0 yr) is the unweathered glacial sediment that can be found either at the glacier front or below the soils (C horizon). The unweathered parent material used for the optical investigations was collected at the bottom of the excavated profiles or glacial front (n = 7 C horizon samples were considered). The soil and parent material samples were oven-dried and sieved to 2 mm (Department of Geography, University of Zurich, Switzerland). An aliquot of the fine earth sample (< 2 mm) was washed with de-ionised water and, when present, the suspended organic fraction (< 1 g/cm^3) was removed by floating. These samples were used for the preparation of thin sections. Fine earth samples (material with a diameter < 2 mm) were dispersed with an ultrasonic disperser, then embedded in polyester resin and cut to a thickness of c. 30 µm in order to ensure a good transparency of the sample. Thin sections were then polished and carbon coated. The grain size of the investigated minerals was in the range of 10 to 800 µm.
In total, > 20 grains were analysed using the Nomarski DIC microscopy or SEM-EDX.

SEM-EDX

The fine-earth fraction of n = 4 topsoil samples and n = 1 parent material were analysed using scanning electron microscopy (SEM) and energy-dispersive spectroscopy (EDS). The analysis was performed using a Dual Beam Quanta 200 3D FEI coupled with EDX, with Dual BSD detector and W emitter operating at an accelerating voltage of 20 kV. The EDS detector is equipped with an ultra-thin window allowing detection of mineral elements and carbon. EDS provided the elemental composition of the solid phases and helped to identify them (point analyses and elemental maps). Investigations were performed on both thin sections (carbon coated) and loose granular samples (uncoated) at the Institute for Building Materials (ETH Zurich, Switzerland).

Cathodoluminescence

Luminescence is a common phenomenon in inorganic and organic compounds, resulting

from an emission transition of anions, molecules or a crystal from an excited electronic state to a ground or other state having less energy (Götze, 2009). In the present study, n = 4 topsoils and n = 1 parent material were investigated. CL measurements were carried out at the Institute of Mineralogyof the TU Bergakademie Freiberg (Germany) using a hot cathode CL microscope HC1-LM (Neuser et al., 1995). The system was operated at 14 kV accelerating voltage and a current density of about 10 μA/mm^2. Luminescence images were taken on-line during CL operations using a Peltier-cooled digital video camera (KAPPA 961-1138 CF 20 DXC). CL spectra were recorded in the wavelength range 320 to 900 nm using an Acton Research SP-2356 digital triple-grating spectrograph with a Princeton Pixi 256B Spec 10 CCD detector that was attached to the CL microscope by a silica-glass fibre guide. CL spectra were measured under standardised conditions (wavelength calibration by a Hg-halogen lamp, spot width 30 μm, measuring time 1–5 s).

Spectral data evaluation was performed considering the relative intensity (counts/s) of the luminescence emission from each sample. The CL spectra depend on the crystal orientation (Barbarand and Pagel, 2001; Finch et al., 2003). Therefore, a comparison of the same mineral type in different samples must be done carefully if the orientation is not the same. Because we were analysing soil systems, a similar orientation of the investigated minerals (in a time series) could not be achieved. A quantitative analysis of weathering in the considered time-span was therefore not possible. To have, however, a semi-quantitative indication for K-feldspar and plagioclase, peaks in the CL spectra were normalised to the Fe peak of the minerals in the parent material and in the soil of interest.

Nomarski DIC microscopy

Nomarski DIC microscopy is a modern technique applied in material science to visualise different phases and/or to image the surface relief of samples (Fig. 2). In the present study, n = 4 topsoils and n = 1 parent material were investigated. The polarisation objectives used have a magnification/numerical aperture of 20x/0.50, 40x/0.75 and 50x/0.80 with specific DIC prisms for transmitted and reflected light studies (Götze, 2009). The microscope was coupled

196 with a digital video camera. The investigations and observations were carried out at the
197 Institute of Mineralogy of the TU Bergakademie Freiberg (Germany).
198
199 *Total element analysis*
200 Element pools in the soil (Ca, Mg, Na, K, Si, Fe, Al, Ti, and Mn) were determined by a total
201 dissolution method for the parental material (average of n = 7 C horizons) and the topsoils
202 having an age > 100 yr (n = 4; Table 2). Oven-dried samples were dissolved using a mixture
203 of HF, HCl, HNO_3, and H_3BO_3 (Hossner, 1996) in a microwave oven and at a pressure of c.
204 25 bar in a closed system. Concentrations were determined by an AAanalyst 600 Perkin
205 Elmer Atomic Absorption Spectrometer (AAS) at the Department of Geography, University of
206 Zurich (Switzerland).
207
208 **Results**
209 The soil mineralogy of the Morteratsch proglacial area has a predominantly silicatic character
210 due to the granitoid parent rock (Mavris et al. 2010, 2011 and Table 2). In the parent material
211 the most abundant phases detected were quartz, K-feldspar and Na-rich plagioclase followed
212 by Fe-rich mica (biotite) and epidote. Apatite was also detected. Furthermore, accessory
213 phases such as pyrite, titanite and ilmenite were detected, but were not the object of this
214 study. Secondary phases due to weathering were almost undetectable. The total
215 concentration of elements remains stable with exposure time (Table 2). The variability is
216 predominantly due to some inhomogeneities of the glacial sediment.
217 The morphology of the minerals is characterised by smooth surfaces and sharp angles –
218 typical for a low weathering degree and limited transport (see Figs. 3 and 4). The amount of
219 rounded grains is low, which is common for morainic material having a minimal chemical
220 leaching and limited transport.
221
222 *Quartz*
223 SEM-EDX. Quartz grains of the parent material have sharp edges and conchoidal surfaces,

typical for short glacial transport. Quartz from the 140 year old soil features a much more uneven surface. The degree of roundness of the grains is higher, and at high magnifications weak traces of chemical corrosion could be detected (Fig. 3). Elemental mapping of quartz grains did not give any evidence of chemical changes following 140 years of weathering, because, apart Si or O, all other elements were below the detection limit of EDS.

CL. The luminescence for the investigated quartz grains was homogeneously dark brown-blue. Primary internal structures (e.g. growth zoning) were usually not observed in the quartz crystals (Fig. 4). CL spectra of quartz indicated some structural changes. The observed broad CL bands of quartz at 450 nm and 650 nm are typical for granitoid-pegmatitic quartz (Richter et al., 2003). The first band represents a defect due to an oxygen vacancy (Stevens Kalceff and Phillips, 1995). The second band is caused by 'nonbridging oxygen hole centres' (NBOHC) (Götze et al., 2001; Fig. 2). A detailed observation of the quartz spectrum of the fresh sediment revealed a small contribution at 620 nm. This is attributed to Si-OH (silanol groups) and becomes hindered by the broad 'NBOHC' band with time (Stevens Kalceff and Phillips, 1995; Fig. 5). In addition, a pronounced band was detected at 710 nm for the quartz of the parent material. This band most likely indicates a substitutional incorporation of Fe^{3+} into the quartz lattice as observed in other silicate structures. This would be typical for the alkali-metasomatic alteration (fenitisation) of the granite (Götze et al., 2001).

Nomarski DIC microscopy. This technique revealed a quite homogeneous morphology for quartz. The rare fractures detected along the surface of the crystals showed that only – if ever – a slight corrosive pre-exposure occurred. In the oldest soil, no clear weathering features were observed.

Feldspar

SEM-EDX. K-feldspar and Na-plagioclase display similar chemical stability with respect to weathering (Allen and Hajek, 1989). Morphologically, we were not able to clearly distinguish the two phases using SEM. In the parent material, the grains appeared to be coarsely-shaped, with sharp, regular cleavage edges, indicating short transport and mechanical

252 abrasion. Across the grain surfaces, a diffuse roughness was observed in both parent
253 material and topsoil samples.
254 CL. The luminescence of K-feldspar showed a blue-violet colour (Fig. 4). Plagioclase showed
255 green luminescence, slightly fading as a function of time. The heterogeneous distribution of
256 CL colours in feldspar minerals indicates weathering/alteration already in the initial rock
257 material. In the CL spectra two emission bands could be observed (Fig. 5). The band at c.
258 460 nm, whose intensity decreases with soil age, is related to Al-O^--Al defects (e.g. Marfunin,
259 1979). The band at c. 680 nm is generated by Fe^{3+} impurities in Al lattice positions (Götze et
260 al., 1999).
261 Nomarski DIC microscopy. Na-plagioclase and K-feldspar exhibited similar features (Fig. 6).
262 Using parallel and crossed Nicols polarised light, the grains revealed surfaces having
263 distinctive, cross-cutting preferential cleavage fissures. Already in the glacial till, two sets of
264 weathering surfaces were distinguishable (Fig. 6). The first one (red arrow) is observed at the
265 outer part of the grain from where the fissures started to penetrate and propagate randomly
266 into the inner part of the mineral grain. The second one (black arrow) developed along
267 parallel sets of cleavage surfaces.
268
269 *Biotite*
270 SEM-EDX. Biotite occurs as layered aggregates with some typical perfect basal cleavages
271 (Fig. 7). In both the parent material and topsoil mechanical deformation and delamination of
272 the layers due to glacial abrasive activity was observed. Furthermore, Ti-containing minerals
273 (titanite?) and feldspar were detected among the mica layers (Fig. 8). SEM-EDX did not
274 evidence a development of secondary phases. In the surface layer and along fissures of the
275 biotite platelets, K appeared depleted compared to Fe due to leaching processes (Fig. 8).
276 CL. Biotite shows a very weak CL intensity because of the quenching by structural iron.
277 Therefore, neither images nor CL spectra were obtained.
278 Nomarski DIC microscopy. Within the weathering sequence, an increasing delamination of
279 biotite with time could be observed. Using the Nomarski technique and SEM, larger spaces

between the mica layers were detectable in the older samples (Fig. 7). As a consequence of the delamination process of mica, a much higher surface area became available for chemical weathering. However, the presence of structurally weaker phases, i.e. newly-formed clay minerals, could not be detected within the biotite platelets. This confirms physical - rather than chemical - alteration of biotite.

Apatite (accessory phase)

SEM-EDX. In the glacial till, apatite was detected as sporadically occurring, euhedral crystals having a size of up to 30 µm. Despite a rather low resistance to weathering in soil profiles having low pH (Allen and Hajek, 1989; Taunton et al., 2000), it was still possible to find apatite crystallites in the oldest topsoil. The EDX measurements did not evidence any significant chemical change in the considered time-span.

CL. Apatite was observed having a strong yellow luminescence emission but did not feature any rim (or growing) structures in the crystal, reflecting a homogeneous composition of apatite (Fig. 4). The CL emission spectra of apatite evidenced sharp emission lines of REE together with a strong Mn^{2+} band at c. 560 nm (Mariano, 1988). A strong enrichment in Ce^{3+}, Nd^{3+}, Sm^{3+} and Eu^{2+} is typical for apatite originating from alkaline magmatic complexes (Zhang et al., 1985; Fleischer and Altschuler, 1986; Mariano, 1988; Boudreau and Kruger, 1990; Kempe and Götze, 2002).

Nomarski DIC microscopy. The detected apatite particles were too small (i.e. < 30 µm) to be properly analysed from a morphological point of view.

Epidote

SEM-EDX. Epidote occurs mainly as elongated crystals having a size of > 50 µm (Fig. 9). In the glacial till, no pre-exposure weathering traces were detected on the epidote crystals. EDX revealed two varieties, a common Fe-rich and a sporadically-occurring REE-bearing epidote (data not shown; see also Mavris et al., 2010). The occurrence of the REE-bearing phases correlates with the dismantlement of pegmatite veins (cf. Büchi, 1994). Epidote did not show

any distinct chemical or mechanical weathering alterations in the oldest topsoil.

CL: Epidote featured a very weak (dark green) luminescence glow. The needle structure of the small crystals, coupled with the strong interfering luminescence of the hosting feldspar did not allow spectral CL measurement of epidote.

Nomarski DIC microscopy. In contrast to SEM-EDX, a distinct epidote alteration was traceable (Fig. 9). Epidote appeared to have a physically and chemically affected crystal structure when compared to the associated (surrounding) phases. The differential interference contrast evidenced this feature where epidote was associated to tectosilicate-structured phases. Neither secondary clay minerals nor oxyhydroxides were observed on the surface of epidote.

Discussion

The collapse of structure bonds is paramount for the transformation of primary tectosilicatic structure into secondary phases (e.g. smectite; Aoudjit et al., 1995). Physical weathering processes (such as freeze-thawing cycles) tend to weaken mineral crystal structures such as large cation-bond tectosilicatic crystal lattices and thus facilitate a further step of elemental leaching by circulating waters (e.g. Hall et al., 2002). The chemical and mineralogical structure of mineral, such as the Fe(II) content, oxygen sharing (the resistance of a primary mineral to weathering increases the degree of sharing of oxygen between adjacent Si tetrahedra in the crystal lattice), lattice distortion etc. strongly determine weathering stability (Curtis, 1976).

In the investigated till, it appears that structural bonds – such as Si-O-Si in quartz – start to break and to transform into free radicals at very early stages of weathering (Figs 3 and 5). This process was also shown in controlled dissolution experiments using quartz (Bennett et al., 1988). The surface of quartz in aqueous solutions consists entirely of species derived from the hydrolysis and hydroxylation of broken =Si-O-Si= and the subsequent protonation and deprotonation of these sites (Furrer and Stumm, 1986; Brady and Walther, 1990). CL spectroscopy was a helpful tool to detect such nano-scale features (Fig. 5). The increase of

both oxygen vacancy and 'NBOHC' bands is the direct consequence of the bond disintegration and a subsequent leaching of Si (or other accessory impurities present, if any). In both, the parent material and the oldest soil of the glacier forefield, the presence of apatite could be verified. Apatite, the main source of inorganic P in the Morteratsch proglacial area, neither displays significant chemical and structural changes nor specific dissolution patterns, even after 140 years of weathering. This is in contrast to the findings of Föllmi et al. (2009b). Their observations of the progressive change in surface morphology of whole apatite grains, the systematic shift in the composition of P phases from detrital to iron-bound and organic P and estimations of the weathering rate of detrital P in the moraine samples indicated that apatite is biogeochemically actively weathered in the proglacial areas of the Rhône and Oberaar glaciers. That we do not observe such a trend in the proglacier area of Morteratsch might be due to a different chemical composition of the apatite or the low number of observations. The CL measurements seem to indicate a weathering of REE in the investigated apatite; however, due to technical constraints, a definitive conclusion is not possible.

The amount of epidote decreased as a function of time (see Mavris et al., 2010). Apparently, the sorosilicate structure of epidote undergoes a leaching of major cations (predominantly Ca^{2+}), thus featuring a chemically-changed crystal lattice (Fig. 9). However, an extended X-ray absorption fine structure (EXAFS) spectroscopy study on Fe in the Damma glacier forefield showed that the Fe fraction within epidote remained constant over the chronosequence (of c. 150 years), indicating a rather low Fe weathering rate of epidote (Kiczka-Cyriac, 2010).

Within the 140 years of weathering the Al-O^--Al bonds of K-feldspar seemed to decrease (Fig. 5) which might be due to a weakening of the crystal structure. Compared to Fe, less Al structural bonds are present in the mineral structure. These structural changes were also confirmed by the Nomarski DIC microscopy (Fig. 6). This reveals remarkable chemical variations most often on the grain surface and at a lattice level. The standardised CL spectra of plagioclase were overwhelmingly overlapping (Fig. 5F) and, consequently, no major

changes could be observed. Finch et al. (2003) reported about a (structurally) ordered plagioclase. The peak ratios after CL excitation/stimulation changed up to 34.3% with the different crystallographic directions of the plagioclase. One way to detect the effective change of specific bonds in a time series is the normalization (ratio) of the band of interest to an 'inert' compound (such as Fe^{3+} in oxic environments). If this ratio varies between two samples more than 34.3%, a real crystallographic change is more likely. If we assume that such a change as a function of orientation is also valid for the plagioclase in the Morteratsch area then no changes can be measured after 140 yr because the peak ratio changes remain below this value. The Al-O^--Al/Fe (460/680 nm) ratio is for 0 years (parent material) = 0.51 and for 140 years = 0.48. The change in the Al-O^--Al/Fe ratio of K-feldspar, however, between 0 years (2.43) and 140 years (1.24) is much higher than one would expect from a spectra-change of the same mineral with varying orientation (according to Finch et al., 2003). Consequently, a part of the Al-O^--Al decrease in the K-feldspar (Fig. 5E, F) must be attributed to weathering (and not only to a change in orientation of the mineral).

Both chemical and physical transformations - namely, elemental depletion of K over Fe, and increased delamination over time - confirmed biotite weathering in the proglacial sediments (Figs 7 and 8). As observed by other authors, biotite typically expands with time, delaminates and contributes to an increase in porosity of the weathered rock (Meunier et al., 2007; Rossi and Graham, 2010; Graham et al., 2010, Caner, 2011). The opening of fissures in mineral grains and the increase in porosity finally give rise to accelerated alteration rates (chemical weathering; Meunier et al., 2007). Fast weathering rates, not only of biotite, can usually be observed at the beginning of soil formation when fresh and reactive surfaces are available (Egli et al., 2003; Mavris et al. 2011). With time, these rates often decrease (Kump et al., 2000; Brantley and Mellott, 2000; Peters, 2009) due to the progressive occlusion of pores by secondary minerals and a decreased chemical potential in the alteration product (Caner, 2011).

The combined CL/Nomarski DIC/ESEM observations of the Morteratsch sediments are based on only a small number of observations. Consequently, our findings cannot be

conclusive and, in particular, more CL measurements on individual minerals are required. The total elemental concentration in the investigated topsoils reveals that the loss of structure-modifying cations within the investigated time span of 140 y is not yet high enough to give rise to a chemical trend along the proglacial area (Table 2). However, on the much smaller atomic and mineral structural scale weathering features can be detected using a combination of CL, Nomarski and SEM-EDX techniques.

Conclusions

Active chemical and physical weathering in a high Alpine chronosequence of recently exposed, granitic sediments could be documented. We have the following main findings:

- Biotite shows distinct mechanical weathering due to delamination of layers within the observed time-span of 140 years.
- Although the bulk chemistry of the soils did not change over time, K-feldspar and Na-plagioclase showed some chemical transformations with respect to Al (K-feldspar) and Mn (plagioclase). SEM-EDX analyses indicated a loss of K in biotite.
- Apatite seemed to be resistant to weathering.
- Epidote, however, shows clear weathering features (such as physical structure disintegration) after 140 years.

The combined use of chemical, mineralogical and spectroscopic analyses proved to be a useful approach in deciphering weathering patterns even at the atomic bond scale (crystal structures). CL and Nomarski DIC have a great potential in detecting and analysing chemical, physical and mineral structural changes due to weathering also in soils. Such an approach should in future enable a qualitative and semi-quantitative estimation of lattice position losses in primary and accessory minerals.

Acknowledgements

This research was supported by the Swiss National Foundation (SNF) project grant n.

200021-117568 and the SIMP fellowship 2009 (SIMP, Italian Society for Mineralogy and Petrology, Italy). We would like to thank G. Peschke and F. Favilli for the help during field-work and in the laboratory. We are furthermore indebted to Dr. Carita Augustsson, Dr. Sergio Andò and the editorial staff of Sedimentary Geology for the fruitful comments to a previous version of the manuscript.

References

Aoudjit, H., Robert, M., Elsass, F., Curmi, P., 1995. Detailed study of smectite genesis in granite saprolites by analytical electron microscopy. Clay Minerals 30, 135-148.

Allen, B.L., Hajek, B.F., 1989. Mineral occurrence in soil environments. In: Dixon, J.B., Weed, S.B. (eds.) Minerals in Soil Environments. SSSA Book Series 1, 199-278.

Anderson, S.P., Drever, J.I., Humphrey, N.F., 1997. Chemical weathering in glacial environments. Geology 25, 399-402.

Anderson, S.P., Drever, J.I., Frost, C.D., Holden, P., 2000. Chemical weathering in the foreland of a retreating glacier. Geochimica et Cosmochimica Acta, 64, 1173-1189.

Barbarand, J., Pagel, M., 2001. Cathodoluminescence study of apatite crystals. American Mineralogist 86, 473-484.

Bennett, P. C., Siegeld, I., Melcerm, E., Bassett, J. P., 1988. The dissolution of quartz in dilute aqueous solutions of organic acids at 25°C. Geochimica et Cosmochimica Acta 52, 1521-1530.

Boudreau, A.E., Kruger, F.J., 1990. Variation in the composition of apatite through the Merensky cyclic unit in the Western Bushveld Complex. Economic Geology 85, 737-745.

Brady, P.V. and Walther, J.V., 1990. Quartz dissolution at low temperature. Chemical Geology 82, 253-264.

Brantley, S.L., Mellott, N., 2000. Surface area and porosity of primary silicate minerals. American Mineralogist, 85, 1767-1783.

nden,

Schweiz). Schweizerische Mineralogische und Petrographische Mitteilungen 74, 359-371.

448 Burga, C., 1999. Vegetation development on the glacier forefield Morteratsch (Switzerland).
449 Applied Vegetation Science 2, 17-24.
450 Caner, L., 2011. Phyllosilicates des sols: de l'altération à la quantification. Habilitation,
451 University of Poitiers, France.
452 Curtis, C. D., 1976. Stability of minerals in surface weathering reactions: A general
453 thermochemical approach. Earth Surface Processes 1, 63-70.
454 D'Amico, C., Innocenti, F., Sassi, F. P., 1998. Magmatismo e Metamorfismo. Ed. UTET,
455 Torino.
456 Egli, M., Mirabella, A., Fitze, P., 2003. Formation rates of smectites derived from two
457 Holocene chronosequences in the Swiss Alps. Geoderma 117, 81-98.
458 Finch, A.A., Hole, D.E., Townsend, P.D., 2003. Orientation dependence of luminescence in
459 plagioclase. Physics and Chemistry of Minerals 30, 373-381.
460 Fleischer, M., Altschuler, Z.S., 1986. The lanthanides and yttrium in minerals of the apatite
461 group: an analysis of the available data r Mineralogie Monatshefte
462 10, 467-480.
463 Föllmi, K.B., Arn, K., Hosein, R., Adatte, T., Steinmann, P., 2009a. Biogeochemical
464 weathering in sedimentary chronosequences of the Rhône and Oberaar Glaciers (Swiss
465 Alps): rates and mechanisms of biotite weathering. Geoderma 151, 270-281.
466 Föllmi, K.B., Hosein, R., Arn, K., Steinmann, P., 2009b. Weathering and the mobility of
467 phosphorus in the catchments and forefields of the Rhône and Oberaar glaciers, central
468 Switzerland: Implications for the global phosphorus cycle on glacial-interglacial
469 timescales. Geochimica et Cosmochimica Acta 73, 2252-2282.
470 Furrer, G., Stumm, W., 1986. The coordination chemistry of weathering: I. Dissolution
471 kinetics of δ-Al_2O_3, and BeO. Geochimica et Cosmochimica Acta 50, 1847- 1860.
472 Götze, J., Habermann, D., Neuser, R. D., Richter, D. K., 1999. High-resolution spectrometric
473 analysis of rare earth elements-activated cathodoluminescence in feldspar minerals.
474 Chemical Geology 153, 81-91.
475 Götze, J., Krbetschek, M.R., Habermann D., Wolf, D., 2000. High-resolution

476 cathodoluminescence studies of feldspar minerals. In: Pagel, M., Barbin, V., Blanc P.,
477 Ohnenstetter, D. (Eds.), Cathodoluminescence in Geosciences, Springer, Berlin, 245–
478 270.
479 Götze, J., Zimmerle, W., 2000. Quartz and silica as guide to provenance in sediments and
480 sedimentary rocks. Contributions to Sedimentary Geology 12, 1-91.
481 Götze, J., Plötze, M., Habermann, D., 2001. Origin, spectral characteristics and practical
482 applications of the cathodoluminescence (CL) of quartz – a review. Mineralogy and
483 Petrology 71, 225-250.
484 Götze, J., Plötze, M., Graupner, T., Hallbauer, D. K., Bray, C. J., 2004. Trace element
485 incorporation into quartz: A combined study by ICP-MS, electron spin resonance,
486 cathodoluminescence, capillary ion analysis, and gas chromatography. Geochimica et
487 Cosmochimica Acta 68, 3741- 3759.
488 Götze J, Siedel H., 2004. Microscopic scale characterization of ancient building sandstones
489 from Saxony (Germany). Material Characterization 53, 209–222.
490 Götze J, Siedel H., 2007. A complex investigation of building sandstones from Saxony
491 (Germany). Material Characterization 58, 1082–1094.
492 Götze, J., 2009. Application of Nomarski DIC and cathodoluminescence (CL) microscopy to
493 building material. Material Characterization 60, 594-602.
494 Graham, R.C., Rossi, A.M., Hubbert, K.R., 2010. Rock to regolith conversion: Producing
495 hospitable substrates for terrestrial ecosystems. GSA Today 20, 4-9.
496 Haeberli, W., Beniston, M., 1998. Climate change and its impacts on glaciers and permafrost
497 in the Alps. Ambio, 27, 258-265.
498 Hall, K., Thorn, C.E., Matsuoka, N., Prick, A., 2002. Weathering in cold regions: some
499 thoughts and perspectives. Progress in Physical Geography 26, 577-603.
500 Hosein, R., Arn, K., Steinmann, P., Adatte, T., Föllmi, K.B., 2004. Carbonate and silicate
501 weathering in two presently glaciated, crystalline catchments in the Swiss Alps.
502 Geochimica et Cosmochimica Acta 68, 1021-1033.
503 Hossner, C.R., 1996. Dissolution for total elemental analysis. In: Sparks, D.L. (Ed.), Methods

of Soil Analysis, Part 3, Chemical Methods. Soil Science Society of America Inc. and American Society of Agronomy Inc., Madison, WI, 49–64.

IUSS Working Group WRB, 2006. World Reference Base for Soil Resources 2006, 2nd edition, World Soil Resources Reports No. 103, FAO (Food and Agriculture Organisation of the United Nations), Rome.

Keevil, C.W., Walker J., 1992. Nomarski DIC microscopy and image analysis of biofilms. Binary Computational Microbiology 4, 93–95.

Kempe, U., Götze, J., 2002. Cathodoluminescence (CL) behaviour and crystal chemistry of apatite from rare-metal deposits. Mineralogical Magazine 66, 151-172.

Kiczka-Cyriac, M., 2010. Iron isotope fractionation mechanisms of silicate weathering and iron cycling by plants. Ph.D. thesis, ETH Zurich.

Kump, L.R., Brantley, S.L., Arthur, M.A. 2000. Chemical weathering, atmospheric CO_2, and climate. Annual Review Earth & Planetary Sciences, 28, 611-617.

Lapuente, M.P., Turi, B., Blanc, P., 2000. Marbles from Roman Hispania: stable isotope and cathodoluminescence characterization. Applied Geochemistry 15, 1469–93.

Marfunin, A.S., 1979. Spectroscopy, luminescence and radiation centers in minerals. Springer-Verlag, Berlin.

Mariano, A.N., 1988. Some further geological applications of cathodoluminescence. In: Marshall, D.J. (ed.), Cathodoluminescence of Geological Materials. Unwin Hyman, Boston, USA, 94-123.

Mavris, C., Egli, M., Plötze, M., Blum, J.D., Mirabella, A., Giaccai, D., Haeberli, W., 2010. Initial stages of weathering and soil formation in the Morteratsch proglacial area (Upper Engadine, Switzerland). Geoderma 155, 359-371.

Mavris, C., Plötze, M., Mirabella, A., Giaccai, D., Valboa, G., Egli, M., 2011. Clay mineral evolution along a soil chronosequence in an Alpine proglacial area. Geoderma 165, 106-117.

Meunier, A., Sardini, P., Robinet, J.C., Prêt, D. 2007. The Petrography of weathering processes. Facts and outlooks. Clay Minerals 42, 415-435.

532 Michalski, S.T., Götze, J., Siedel, H., Magnus, M., Heimann, R.B., 2002. Investigations into
533 provenance and properties of ancient building sandstones of the Zittau/Görlitz region
534 (Upper Lusatia, Eastern Saxony, Germany). In: Siegesmund, S., Vollbrecht, A., Weiss, T.,
535 (Eds.), Natural stone, weathering phenomena, conservation strategies and case studies.
536 Special Publications, vol. 205. London: Geological Society, pp. 281–295.
537 Murphy, S.F., Brantley, S.L., Blum, A.E., White, A.F., Dong, H., 1998. Chemical weathering
538 in a tropical watershed, Luquillo Mountains, Puerto Rico: II. Rate and mechanism of biotite
539 weathering. Geochimica et Cosmochimica Acta 62, 227–243.
540 Neuser, R.D., Bruhn, F., Gätze, F., Haberman, J., Richter, D.K., 1995. Kathodolumineszenz:
541 Methodik und Anwendung. Zentralblatt für Geologie und Paläontologie Teil 1, 287-306.
542 Nomarski, G., Weill, A.R., 1951. Sur l'observation des figures de croissance des cristaux par
543 les methods interférentielles à deux ondes. Société française de Minéralogie et de
544 Cristallographie Bulletin 77, 840–868.
545 Nomarski, G., 1955. Microinterféromètre differentiell a ondes polarisées. Journal de Le
546 Physique et Le Radium 16, 9–13.
547 Pearce, T.H., Russell, J.K., Wolfson, I., 1987. Laser-interference and Nomarski interference
548 imaging of zoning profiles in plagioclase phenocrysts from the May 18, 1980, eruption of
549 Mount St. Helens, Washington. American Mineralogist 72, 1131–1143.
550 Peters, C. A. 2009. Accessibilities of reactive minerals in consolidated sedimentary rock: An
551 imaging study of three sandstones. Chemical Geology 265, 198-208.
552 Richter, D.K., Götte, T., Götze, J., Neuser R.D., 2003. Progress in application of
553 cathodoluminescence (CL) in sedimentary petrology. Mineralogy and Petrology 79, 127-
554 166.
555 Rossi, A. M., Graham, R.C., 2010. Weathering and Porosity Formation in Subsoil Granitic
556 Clasts, Bishop Creek Moraines, California. Soil Science Society of America Journal 74,
557 172-185.
558 Stevens Kalceff, M.A., Phillips, M.R., 1995. Cathodoluminescence microcharacterization of
559 the defect structure of quartz. Physical Review 52, 3122-3135.

560 Swoboda-Colberg, N.G., Drever, J.I., 1993. Mineral dissolution rates in plot-scale field and
561 laboratory experiments. Chemical Geology 105, 51–69.
562 Taunton, A.E., Welch, S.A., Banfield, J.F., 2000. Microbial control on phosphate and
563 lanthanide distributions during granite weathering and soil formation. Chemical Geology
564 169, 371-382.
565 Trommsdorff, V., Dietrich, V., 1999. Grundzüge der Erdwissenschaften. 6th edition, vdf-
566 Verlag, Zürich, Switzerland.
567 Wadham, J.L., Cooper, R.J., Tranter, M., Hodgkins, R., 2001. Enhancement of glacial solute
568 fluxes in the proglacial zone of a polythermal glacier. Journal of Glaciology 47, 378-386.
569 Yoo, K., Mudd, S.M., 2008. Toward process-based modelling of geochemical soil formation
570 across diverse landforms: A new mathematical framework. Geoderma 146, 248-260.
571 Zhang, S., Wang, L., Yang, W., 1985. Use of REE analysis in apatite to distinguish
572 petrological and mineralogical series of granitic rocks. Geochimica 1, 45-57.

Figure captions

Fig. 1. Overview of the investigated area with the monitored sites in the proglacial area. The isochrones are according to Burga et al. (1999).

Fig. 2. Schematic sketch (modified after Götze, 2009) showing: a) simplified structure of quartz with some typical features detectable using cathodoluminescence (modified after Götze et al., 2001). b) Nomarski DIC microscopy. Optical diagram with the structure of the DIC microscope; bottom: the phase difference (Φ) is explained by geometric (step height 'd') and physical factors (difference in the material specific phase shift 'a' and 'b').

Fig. 3. SEM micrographs with a) quartz grain from the 140 yr old topsoil and b) surface morphology showing an early chemical corrosion of quartz. The arrows point to distinct surface dissolution pits.

Fig. 4. Cathodoluminescence micrographs of apatite, quartz, plagioclase and alkali feldspar of the parent material (0 yr) and 140 yr old topsoil. *Apatite:* yellow luminescing crystals due to the activation of Mn^{2+}; *quartz*: blue-brown CL; *plagioclase*: green luminescing areas with strongly emitting Mn^{2+} peak; *alkali feldspar*: violet emitting grains, related to both Al-O^--Al defects and Fe^{3+} in Al-sites.

Fig. 5. Cathodoluminescence emission spectra of A) quartz, B) alkali feldspar, C) plagioclase and D) apatite. The bold line denotes the 140 yr topsoil and the thin line the parent material. The spectra E (alkali feldspar) and F (plagioclase) are normalised to the Fe-spectrum of the parent material.

Fig. 6. Plagioclase from the parent material (0 yr) and the 140 yr old topsoil. In the parent material, two sets of weathering patterns are underlined: geologically inherited (along cleavage surfaces; red arrows), and pedogenic (mostly on the outer surface of the grains; black arrow). The image shows the grains in thin section in parallel and crossed Nicols transmitted (polarised) light.

Fig. 7. (*above*) Delamination of biotite crystallites in the parent material (t = 0 yr) and in the oldest topsoil (t = 140 yr) observed using SEM; (*below*) biotite delamination as a function of the time documented using Nomarski DIC microscopy.

Fig. 8. Elemental mapping (SEM-EDX) of K and Fe in biotite of the parent material and the oldest soil.

Fig. 9. Micrographs of epidote from the parent material (0 yr) and the oldest topsoil aged (140 yr). The image shows the grains in thin section in parallel and crossed Nicols transmitted (polarised) light.

Figure 1

Click here to download high resolution image

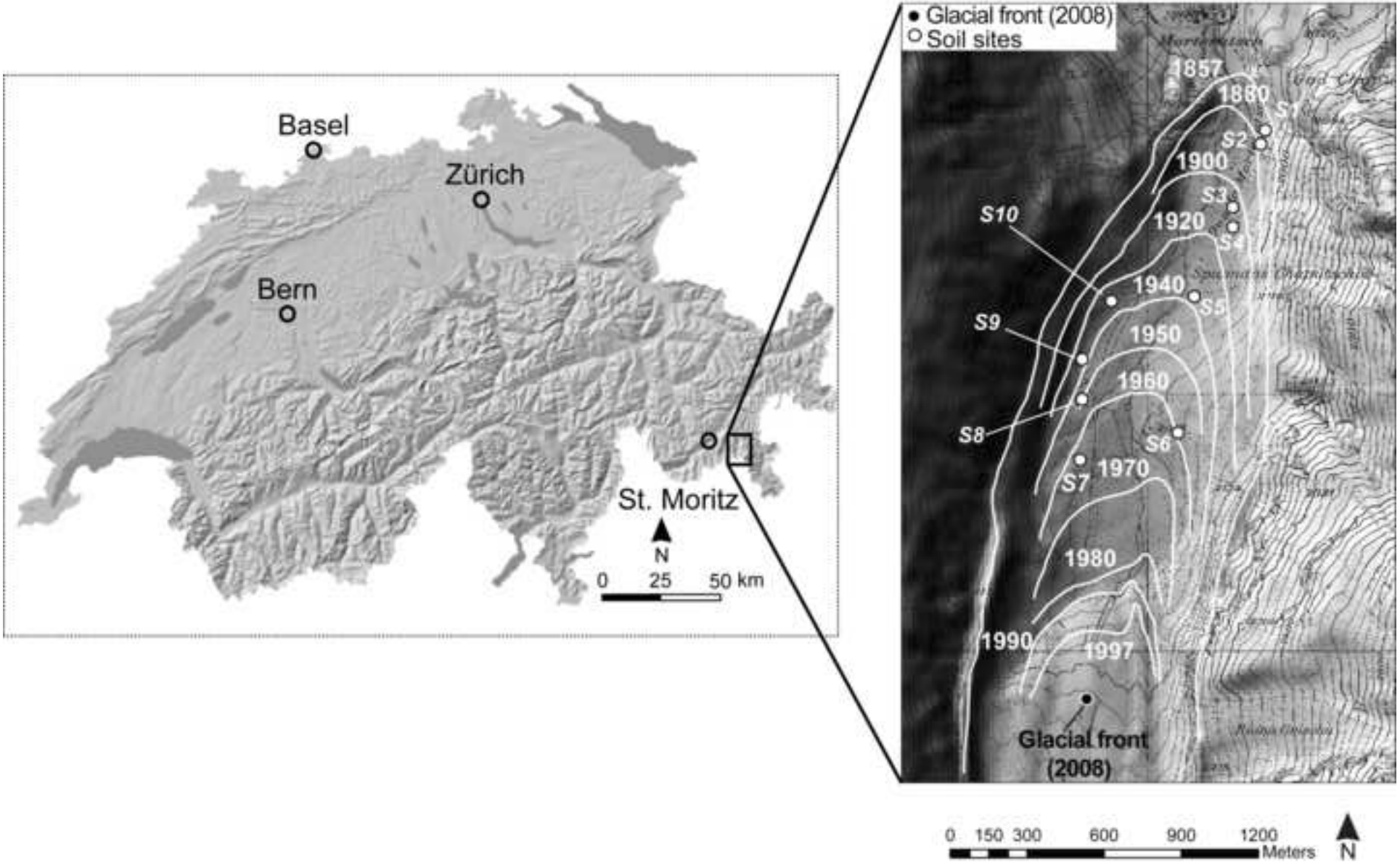

Figure 2

Click here to download high resolution image

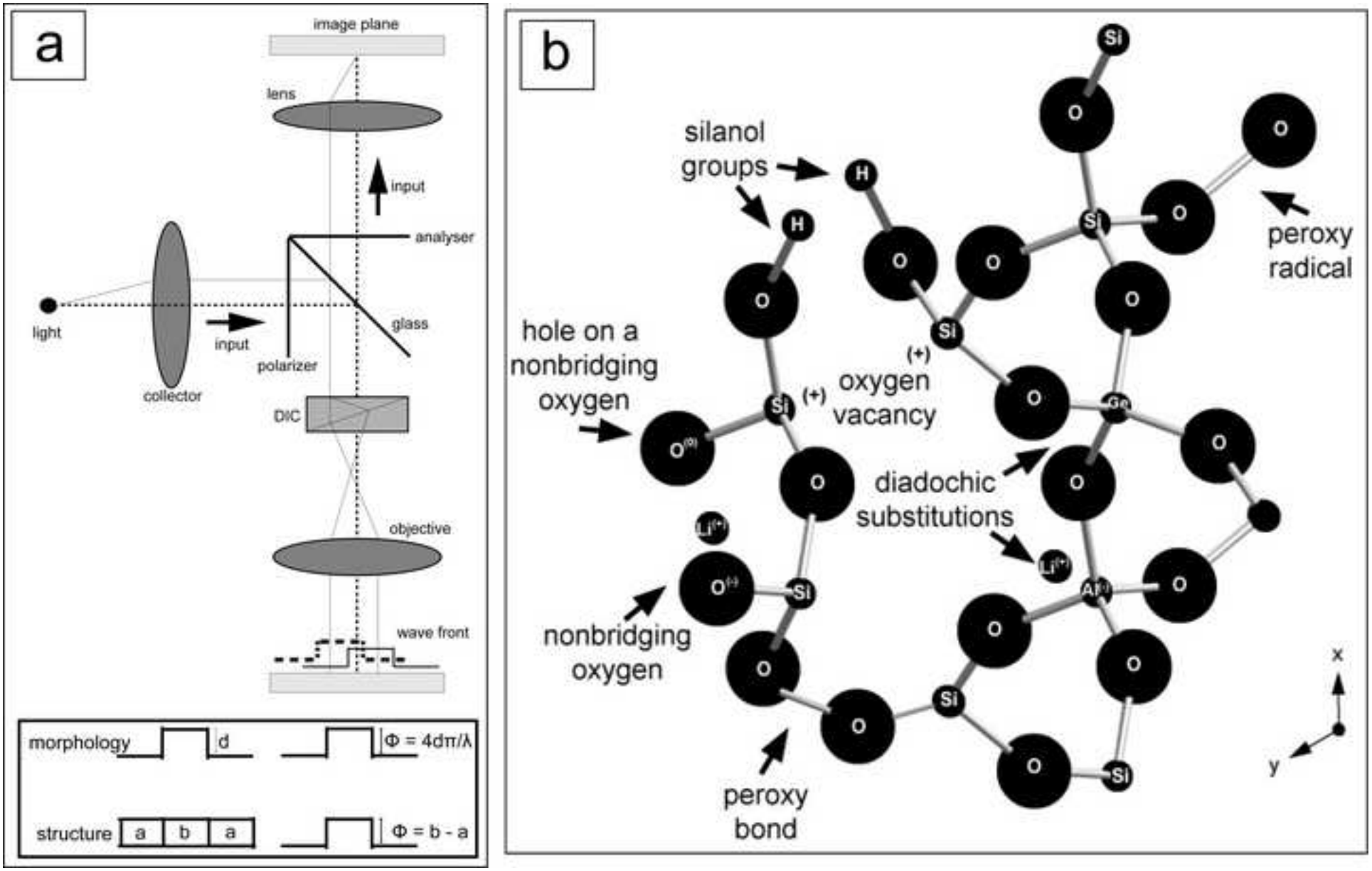

Figure 3

Click here to download high resolution image

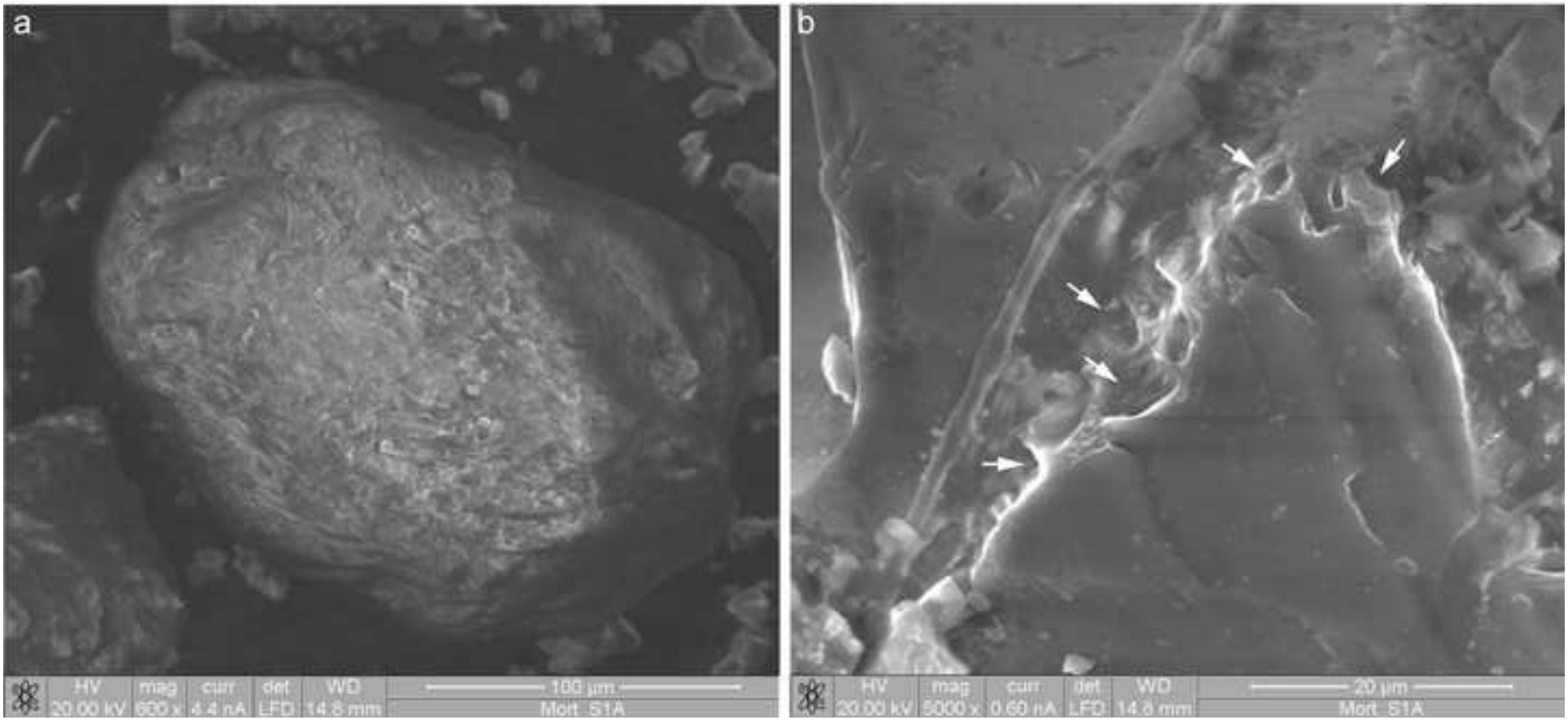

Figure 4

Click here to download high resolution image

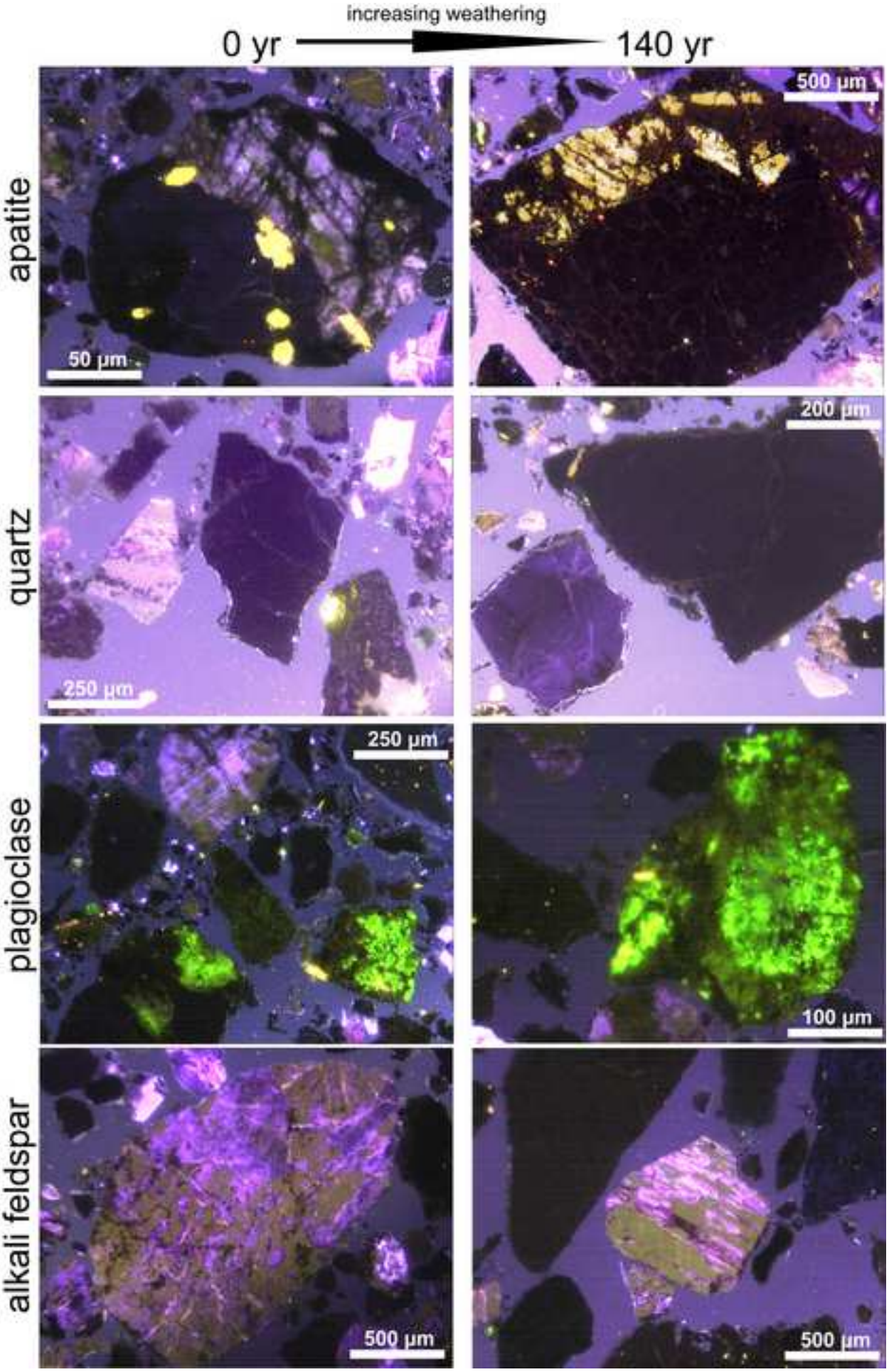

Figure 5

Click here to download high resolution image

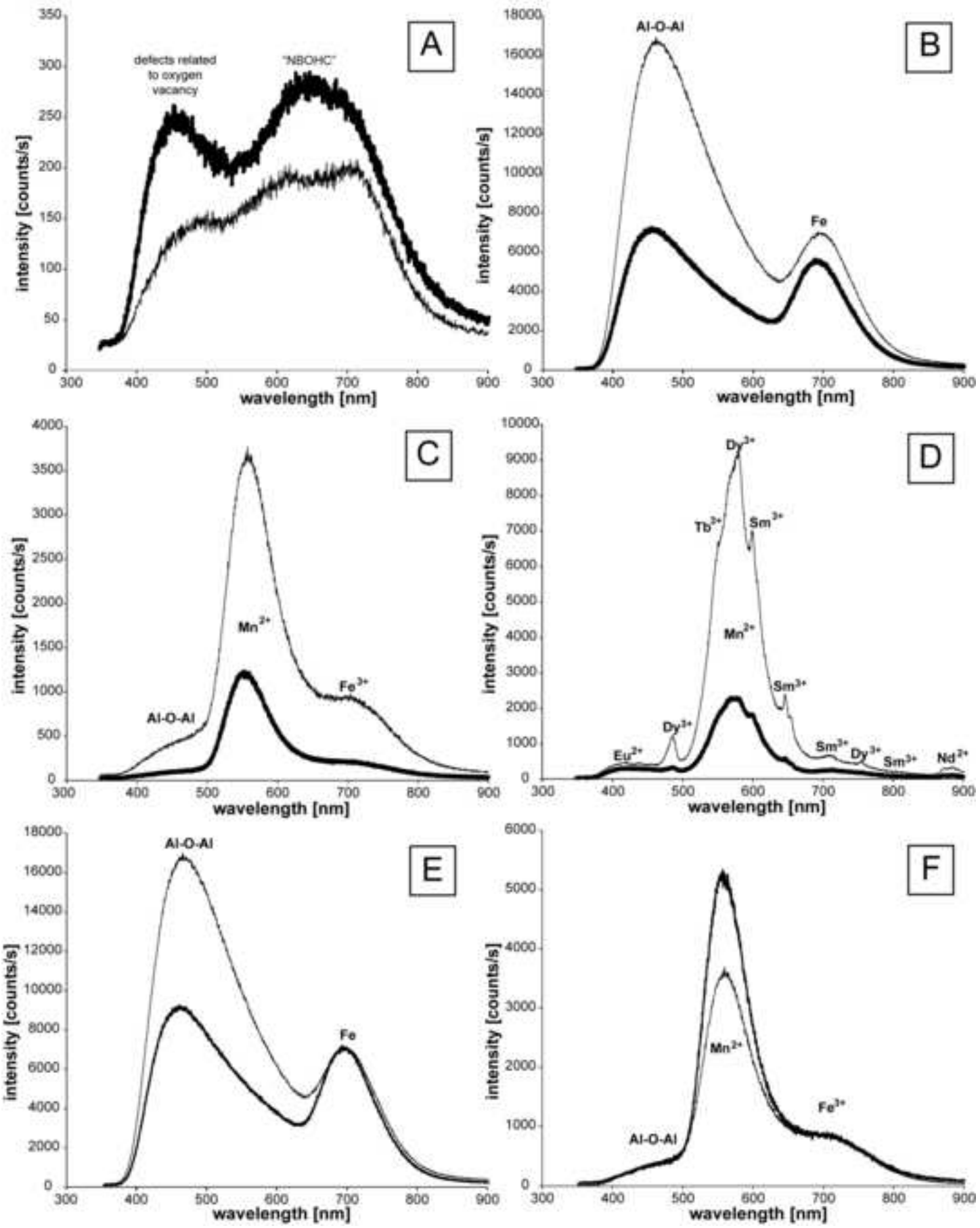

Figure 6

Click here to download high resolution image

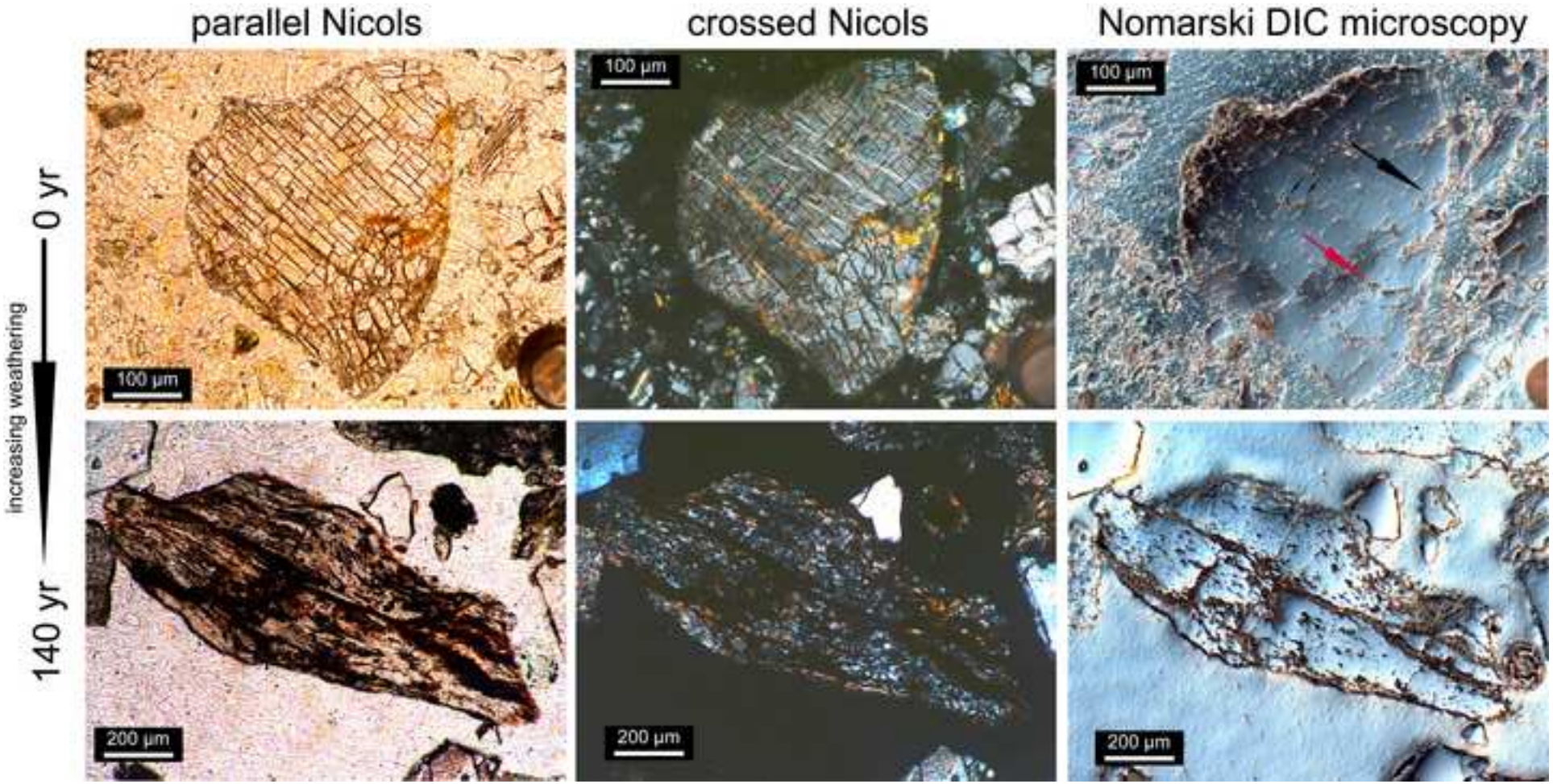

Figure 7

Click here to download high resolution image

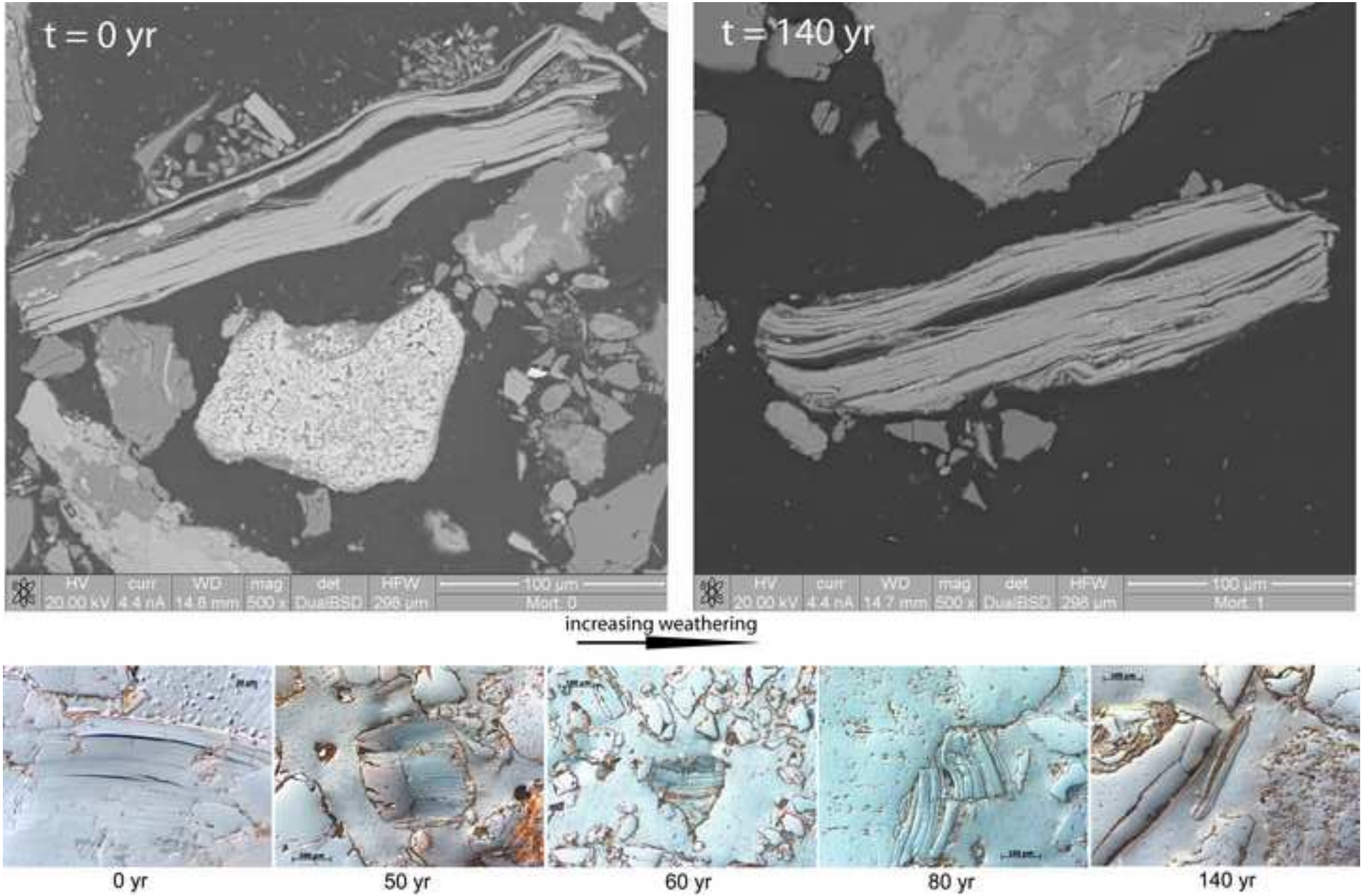

Figure 8

Click here to download high resolution image

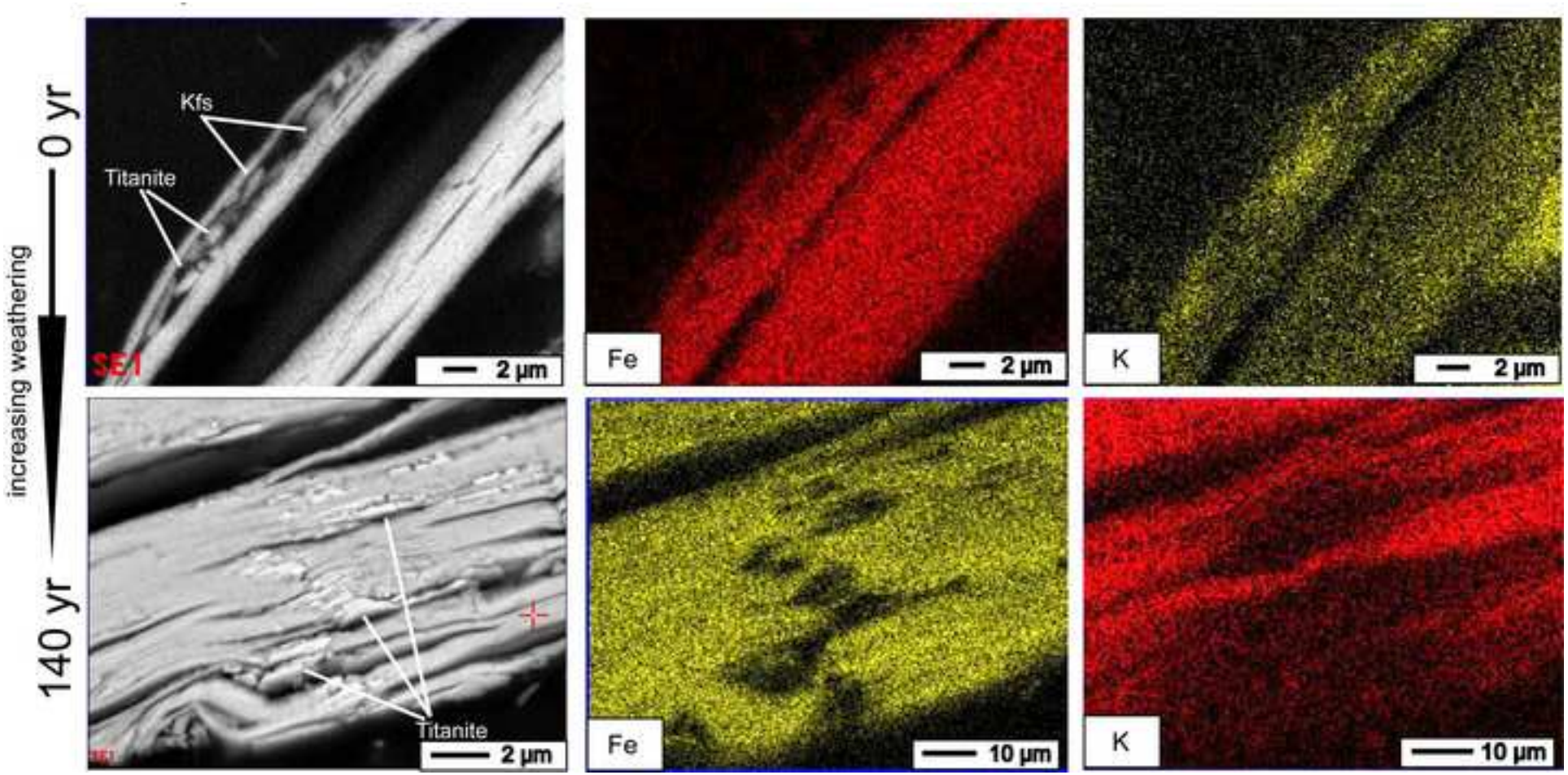

Figure 9

Click here to download high resolution image

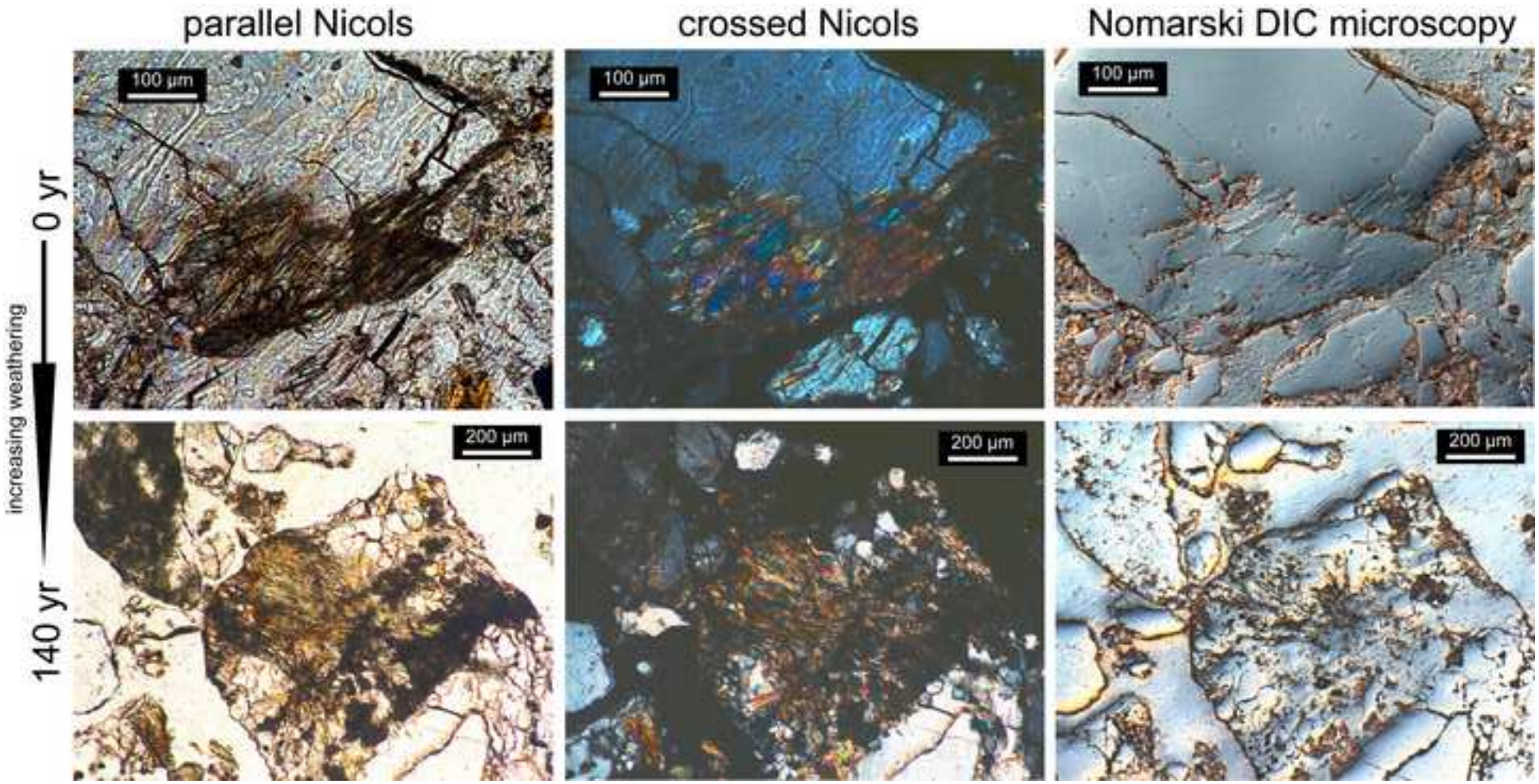

Table 1
Click here to download Table: Table1.doc

Table 1. Properties of the monitored soil sites. Grain sizes: sand (2000-63 μm), silt (63-2 μm) and clay (< 2 μm).

Site/Soil	Soil age (yr)	Horizons	Depth (cm)	Skeleton (wt. - %)	Sand (g/kg)	Silt (g/kg)	Clay (g/kg)	pH ($CaCl_2$)
S1/Humi-Skeletic Leptosol	138	O	0-6	41	n.m.	n.m.	n.m.	4.60
		A	6-9	50	777	184	39	4.80
		BC	9-14	53	830	158	12	4.70
		C	14-30	40	757	222	21	4.60
S2/Humi-Skeletic Leptosol	128	A	0-10	64	754	204	42	4.85
		AC	10-40	68	695	272	33	4.90
S3/Humi-Skeletic Leptosol	108	A	0-3	54	667	265	68	5.10
		AC	3-15	70	677	281	42	4.50
S4/Humi-Skeletic Leptosol	98	A	0-1	55	n.m.	n.m.	n.m.	5.30
		AC	1-5	51	939	61	15	5.20
		C	5-30	70	931	57	12	5.20
S5/Humi-Skeletic Leptosol	68	A1	0-1	7	n.m.	n.m.	n.m.	4.85
		A2	1-4	1	530	432	38	4.55
		C1	4-9	36	573	387	40	4.65
		C2	9-20	64	570	372	58	4.60
S6/Skeletic Leptosol	48	A	0-2.5	64	n.m.	n.m.	n.m.	4.80
		C	2.5-25	68	852	129	19	5.00
S7/Skeletic Leptosol	48	A	0-4	26	n.m.	n.m.	n.m.	6.10
		C1	4-11	37	823	146	31	5.20
		C2	11-34	67	747	211	42	5.10
S8/Skeletic Leptosol	58	OA	0-12	63	n.m.	n.m.	n.m.	4.60
		C	12-33	48	712	220	68	4.40
S9/Humi-Skeletic Leptosol	73	O	0-3	44	n.m.	n.m.	n.m.	5.15
		AC	3-10	65	785	175	40	4.40
		C	10-36	58	832	133	35	4.65
S10/Humi-Skeletic Leptosol	78	A1	0-2	49	n.m.	n.m.	n.m.	4.70
		A2	2-10	68	818	143	39	4.50
		AC	10-25	84	733	219	48	4.80

n.m. = not measured

Table 2. Total chemical analysis of the > 100 yr topsoils (n = 4) and the parent material (n = 7) with standard deviation (SD).

	Al (g/kg)	Si (g/kg)	Ti (g/kg)	Ca (g/kg)	Mg (g/kg)	K (g/kg)	Na (g/kg)	Fe (g/kg)	Mn (g/kg)
parent material	76.8	310.2	8.00	17.2	9.53	28.7	26.8	22.5	0.58
SD	6.5	27.4	2.38	6.4	3.20	4.1	3.87	6.9	0.16
topsoils (age >100 yr)	65.0	330.4	5.90	27.3	7.32	28.1	25.3	29.1	0.62
SD	5.8	24.0	2.25	22.3	2.77	2.4	2.6	16.1	0.14